Vol. 60: 215–234, 2014
doi: 10.3354/cr01239

CLIMATE RESEARCH
Clim Res

Published August 5

Assessment of RegCM4.3 over the CORDEX South America domain: sensitivity analysis for physical parameterization schemes

Michelle Simões Reboita[1], Julio Pablo R. Fernandez[2], Marta Pereira Llopart[3], Rosmeri Porfirio da Rocha[3], Luana Albertani Pampuch[3], Faye T. Cruz[4]

[1]Natural Resources Institute, Federal University of Itajubá, Av. BPS, 1303, Itajubá, Minas Gerais, MG 37500-903, Brazil
[2]Center for Weather Forecasting and Climate Research, National Institute for Space Research, Rodovia Presidente Dutra, km 40, Cachoeira Paulista, SP 12630-000, Brazil
[3]Department of Atmospheric Sciences, University of São Paulo, Rua do Matão, 1226, Cid. Universitária, São Paulo, SP 05508-090, Brazil
[4]Regional Climate Systems, Manila Observatory, Loyola Heights, Quezon City 1108, Philippines

ABSTRACT: In mid-2012, the Abdus Salam International Centre for Theoretical Physics (ICTP) released version 4.3 of the Regional Climate Model (RegCM4.3). This version includes a new surface scheme, the Common Land Model (CLM); a new planetary boundary layer (PBL) scheme, the University of Washington PBL (UW-PBL); and new convection schemes including Tiedtke, and Mixed1 and Mixed2 — with Grell (MIT) over the land and MIT (Grell) over the ocean for Mixed1 (Mixed2). These implementations suggest the necessity of an evaluation study to determine the best configuration of RegCM4.3 for simulating the climate of South America (SA). The main motivation is to come up with the best configurations of RegCM4.3 over the SA domain for use in the Coordinated Regional Downscaling Experiment (CORDEX) project. We analyzed 7 simulations for the period 1990–2000. The control simulation used the Biosphere–Atmosphere Transfer Scheme (BATS), Holtslag for the PBL and Mixed1 for cumulus convection. In the other simulations we changed these schemes using the new RegCM4.3 options. The evaluation of the simulations was carried out in 3 groups: (1) sensitivity to convection (Mixed1, MIT and Tiedtke), (2) sensitivity to the PBL (Holtslag and UW-PBL) and (3) sensitivity to surface processes (BATS and CLM). Considering all of SA, the results show that precipitation is better simulated with the schemes of the control simulation, while for air temperature, better results were obtained using the MIT cumulus scheme together with the CLM scheme. In summary, we recommend 2 configurations for the CORDEX project over SA: (1) the schemes used in the control simulation and (2) the MIT scheme for cumulus convection, Holtslag for the PBL, and CLM for surface interaction processes.

KEY WORDS: South America · RegCM4.3 · CORDEX · Simulation · Precipitation · Temperature · Evapotranspiration

1. INTRODUCTION

Regional Climate Models (RCMs) began to be used in the 1990s to improve global model results (Dickinson et al. 1989, Giorgi & Marinucci 1991). According to Sen et al. (2004), the interest in RCMs is due to the greater detail of the physical processes and high spatial resolution that they can achieve, which provides more realistic representation of the local processes affecting the climate. Nowadays, the use of dynamical downscaling is widespread, and allows the outputs of Global Circulation Models (GCMs) or reana-

*Corresponding author: reboita@gmail.com

lysis (e.g. NCEP, ERA-Interim) to be used as initial and boundary conditions in RCMs, for a range of applications. In particular, for South America (SA), RCMs began to be utilized in the 2000s to simulate the observed features of the present climate (Chou et al. 2000, Menéndez et al. 2001, Nobre et al. 2001). The use of RCMs increased in recent years, encompassing objectives such as: investigation of the RCMs' ability to simulate the climate (Nicolini et al. 2002, Seth & Rojas 2003, Fernandez et al. 2006a); the use of different initial and boundary condition forcing (Seth & Rojas 2003, Seth et al. 2007); validation of the simulated diurnal cycle of the precipitation (da Rocha et al. 2009); comparison of the simulated interannual variability of the climate with observations (Misra et al. 2002, Fernandez et al. 2006b, Seth et al. 2007); investigation of the ability of RCMs to simulate specific atmospheric systems climatology (Reboita et al. 2010a); and exploration of future climate scenarios (Nuñez et al. 2009, Marengo et al. 2010, Krüger et al. 2012).

Some studies have pointed out the need for improving the physical parameterizations and assimilation techniques used by RCMs in order to produce a more realistic simulation of the SA climate (Nunes & Roads 2005, Seth et al. 2007, Rauscher et al. 2007). For example, as discussed in da Rocha et al. (2009), Regional Climate Model version 3 (RegCM3; Pal et. al. 2007) simulations show that the convection scheme proposed by Grell (1993) realistically simulates the phase of the diurnal cycle of rainfall and the frequency distribution of daily precipitation, although it underestimates the rainfall intensity over the Amazon. Aiming to improve the representation of precipitation in SA with RegCM3, da Rocha et. al. (2012) changed some parameters of the Biosphere-Atmosphere Transfer Scheme (BATS, Dickinson et. al. 1993) to reduce the water drainage at the bottom of the subsoil layer across the tropical forest, and used a shorter convective time period for the Grell convective scheme (Grell 1993). As a result they found an increase in the intensity of rainfall over the Amazon, with a reduction of the dry bias over the tropics and a better representation of the South American Monsoon (SAM) system. However, these changes had little impact on the intensity of rainfall over the ocean, resulting in rainfall underestimation in the oceanic branch of the South Atlantic Convergence Zone (SACZ) and poor representation of the Intertropical Convergence Zone (ITCZ).

In 2010, the fourth version of the Regional Climate Model (RegCM4; Giorgi et. al. 2012) was launched and in 2012 version 4.3 (RegCM4.3) came out with further improvements. RegCM4.3 includes a new surface scheme, the Common Land Model (CLM; Steiner et al. 2009, Tawfik & Steiner 2011), a new scheme to treat the planetary boundary layer (PBL) physics, called the University of Washington PBL (UW-PBL; Bretherton et al. 2004, O'Brien et al. 2012); the convection scheme of Tiedtke (Tiedtke 1989), and a mixture of 2 convective schemes present in older versions: Grell and MIT, where Mixed1 (Mixed2) has Grell (MIT) over the land and MIT (Grell) over the ocean. The RegCM4.3 parameterizations need to be investigated; it is especially important to know if they can improve the climate simulations in both continental and oceanic areas of SA. Thus, the purpose of this study was to evaluate the performance of RegCM4.3 parameterizations in representing the climate and its variability over SA. We carried out several simulations with different parameterizations for cumulus convection, the PBL, and the soil–plant–atmosphere interaction processes, with the aim of using the best configuration in the Coordinated Regional Downscaling Experiment (CORDEX; Giorgi et al. 2009) project using RegCM4.3 over the SA domain.

2. METHODOLOGY

2.1. RegCM4.3

The basic dynamical component of RegCM4.3 is the same as in RegCM2 (Giorgi et al. 1993a,b) and RegCM3 (Pal et al. 2007), which solves the equations of a compressible atmosphere using finite differences, with hydrostatic balance and a sigma-pressure vertical coordinate. For integration in time, RegCM4.3 uses a split-explicit scheme, in which the fast gravity modes are first separated from the slow modes and then integrated with smaller time steps. RegCM4.3 also has an algorithm to reduce the horizontal diffusion in the presence of steep topographical gradients (Giorgi et al. 1993a,b). A detailed description of the physical parameterization schemes available in RegCM4.3 is presented by Giorgi et al. (2012). We provide here only a summary of the differences in previous and current versions of RegCM.

Planetary boundary layer. According to Giorgi et al. (2012), one of the biggest changes in RegCM4.3 is related to the PBL. The turbulent vertical transfer of the Holtslag (Holtslag et al. 1990) scheme, which has been present since the first version of RegCM, was modified. Another scheme introduced in RegCM4.3 is the UW-PBL that is based on the general turbu-

lence closure parameterization of Grenier & Bretherton (2001) and Bretherton et al. (2004). The UW-PBL was introduced in RegCM4.3 to improve the simulation of the stratocumulus sheet at the top of the PBL that is normally observed in western North America (O'Brien et al. 2012).

Cumulus convection. RegCM4.3 has 6 options for cumulus convection: Kuo (Anthes 1977, Anthes et al. 1987), Grell (1993), MIT (Emanuel 1991, Emanuel & Zivkovic-Rothman 1999), Tiedtke (1989), Mixed1 (Grell over the land and MIT over the ocean) and Mixed2 (Grell over the ocean and MIT over the land). Tiedtke, Mixed1 and Mixed2 schemes are the new options in RegCM4.3. In the Kuo scheme convection is triggered in a convectively unstable low troposphere when the column moisture convergence exceeds a threshold value (Giorgi et al. 2012). However, this scheme produces very dry conditions over SA (Reboita et al. 2013) and therefore it was not used in this study. The Grell scheme was implemented for Giorgi et al. (1993b) and it is the most commonly used scheme in RegCM simulations. In this scheme clouds are considered as 2 steady-state circulations including an updraft and a penetrative downdraft. Convection is activated after a parcel lifted in the updraft reaches the level of moist convection (Giorgi et al. 2012). Two types of closures can be adopted in the Grell scheme, such that either all buoyant energy is immediately removed at each time step (Arakawa-Schubert type closure) or it is released during a time period of the order of 30 min (Fritsch-Chappell type closure; Pal et al. 2007). The MIT scheme (Emanuel 1991, Emanuel & Zivkovic-Rothman 1999) was introduced in RegCM3 (Pal et al. 2007) and it considers that convection is activated when the level of buoyancy is higher than the cloud base level. The convective scheme of Tiedtke (1989) considers a population of clouds where the cloud ensemble is described by a one-dimensional bulk model. One of the major differences with respect to convection between RegCM4.3 and its past versions is the possibility of using one convective scheme over ocean and other one over continent at the same time. Many tests conducted by Giorgi et al. (2012) showed that different schemes perform differently over land and ocean areas. Thus, the 2 mixed schemes are available in RegCM4.3, i.e. Mixed1 and Mixed2.

Land surface. Land surface processes in RegCM4.3 have been described by the Biosphere–Atmosphere Transfer Scheme (BATS) of Dickinson et al. (1993). BATS is a 'second-generation' land surface model, which uses a force-restore method to calculate soil temperature, has 3 soil layers for interactive soil moisture calculations, 1 bulk snow layer, 1-layer vegetation, and a simple description of surface runoff (Giorgi et al. 2012). RegCM4.3 has the Community Land Model (CLM3.5) as an option. The CLM3.5 is a state-of-the-science land surface parameterization developed and supported by NCAR (Oleson et al. 2004, 2008). CLM3.5 is a 'fourth-generation' land surface model, in that it includes a physical representation of the coupling between the water, energy and carbon cycles (Sellers et al. 1997). A detailed description of the differences between BATS and CLM is presented in Steiner et al. (2005), Steiner et al. (2009) and Tawfik & Steiner (2011).

2.2. Data and design of the simulations

The domain of the simulations (Fig. 1) is the same as that used in da Rocha et al. (2012) and follows the CORDEX recommendation for SA (Giorgi et al. 2009). This domain has 192 × 202 grid points in the north–south and west–east directions, respectively, with a horizontal grid spacing of ~50 km and 18 sigma-pressure levels in the vertical. The simulations

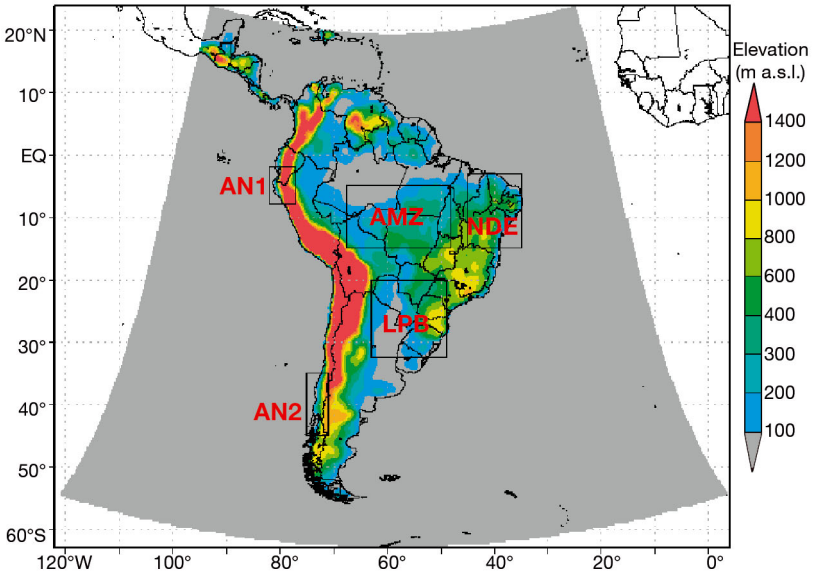

Fig. 1. Domain of the simulations (gray shading) and subdomains used to validate the experiments: Amazonia (AMZ), northeastern Brazil (NDE), La Plata Basin (LPB), Andean region over the border between Ecuador and Peru (AN1) and Andean region over southern Chile (AN2)

used the Mercator-rotated projection and were driven by atmospheric variables (geopotential height, temperature, wind and relative humidity) from the ERA-Interim reanalysis (Dee et al. 2011). This reanalysis dataset has 1.5° horizontal resolution with 37 pressure levels in the vertical. The NOAA optimum interpolation (OI) sea surface temperature V2 weekly means (Reynolds et al. 2002), with a 1.0° horizontal resolution, was also used in the simulations. The topography and land use data were specified by using 10′ horizontal resolution global archives from the United States Geological Survey (USGS) and Global Land Cover Characterization (GLCC), respectively, which are described by Loveland et al. (2000).

We carried out 7 simulations with RegCM4.3 for the period from January 1, 1989 to January 1, 2000 (Table 1). The first simulation year is considered as a spin-up period, and hence excluded from the analyses. The control simulation (S_CTRL) follows the Giorgi et al. (2012) specifications: BATS surface scheme, Holtslag PBL scheme and the Mixed1 cumulus convection parameterization. The details for the other simulations are listed in Table 1. In all simulations, the ocean fluxes were parameterized with the Zeng scheme (Zeng et al. 1998), which provides realistic climatology of latent heat fluxes over the South Atlantic Ocean (Reboita et al. 2010b).

Model results for precipitation and air temperature were validated against gridded observational datasets. For precipitation, we have used the monthly climatology of the Climate Prediction Center Merged Analysis of Precipitation (CMAP; Xie & Arkin 1997) and the Climate Research Unit (CRU; Brohan et al. 2006) dataset. Air temperature data were obtained from CRU and Delaware University (UDEL, Legates & Willmott 1990). CMAP is available over the whole globe with 2.5° horizontal resolution while CRU and UDEL are available only over continents with finer horizontal grid (0.5° × 0.5° longitude by latitude). We also carried out objective comparisons between simulations and analyses (CMAP, CRU and UDEL) using statistical indices (bias, Pearson correlation coefficient and standard deviation, SD) calculated in the 5 subdomains indicated in Fig. 1: Amazonia (AMZ), northeastern Brazil (NDE), La Plata Basin (LPB), Peru-Ecuador border (AN1) and southern Chile (AN2). In

Table 1. Setup of RegCM4.3 simulations. ibltyp: PBL scheme code; atwo: efficiency of enhancement of entrainment by cloud evaporation; icup: cumulus convection scheme code; entrpen: entrainment rate for penetrative convection; cmtcape: CAPE adjustment timescale parameter; ctrigger: trigger parameter; elcrit: autoconversion threshold water content (g/g) and coeffr: coefficient governing the rate of rain evaporation

Simulations	Physical schemes		
	Surface scheme	Boundary layer	Cumulus convection
S_CTRL	BATS	Holtslag et al. (1990) ibltyp = 1	Mixed1: Grell over land and Emanuel over ocean icup = 99
S_Tiedtke	BATS	Holtslag et al. (1990) ibltyp = 1	Tiedkte (1989) icup = 5 Modifications: entrpen = 1.0D-4 to 0.5D-4 cmtcape = 40.0D0 to 20.0D0 ctrigger = –1.1D01
S_MIT	BATS	Holtslag et al. (1990) ibltyp = 1	Emanuel (1991) icup = 4 Modification elcrit = 0.011D0 to 0.00011D0, coeffr = 1.0D0 to 2.0D0
S_PBL	BATS	UW-PBL (Bretherton et al. 2004): Ibltyp = 2 Modification atwo = 15.0D0 to atwo = 10.0D0	Mixed1: Grell over land and Emanuel over ocean icup = 99
S_PBL_MIT	BATS	UW-PBL (Bretherton et al. 2004): Ibltyp = 2 Modification atwo = 15.0D0 to atwo = 10.0D0	Emanuel (1991) icup = 4
S_CLM	CLM	Holtslag et al. (1990) ibltyp = 1	Mixed1: Grell over land and Emanuel over ocean icup = 99
S_CLM_MIT	CLM	Holtslag et al. (1990) ibltyp = 1	Emanuel (1991) icup = 4 Without modifications

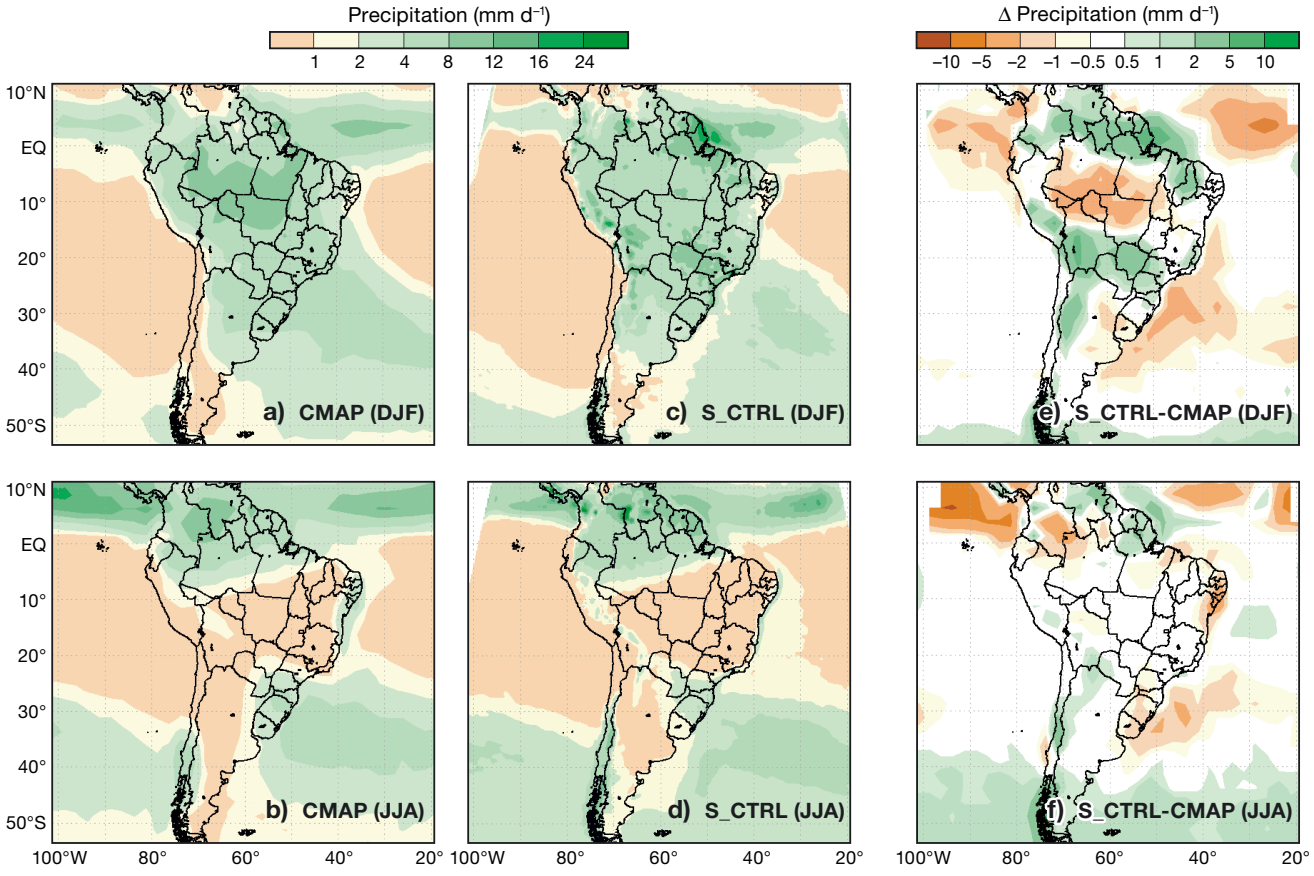

Fig. 2. Mean precipitation (1990–1999) in (a,c) DJF and (b,d) JJA from CMAP and S_CTRL, and (e,f) difference between datasets (S_CTRL-CMAP) in each season

these areas, the SD and correlation were calculated for the seasonal time series to obtain a measure of the ability of RegCM4.3 to simulate the observed interannual variability.

The simulated surface energy partitioning over the Amazon region simulated by S_CTRL, S_MIT and S_CLM_MIT was evaluated using the Bowen Ratio (β; Bowen 1926). β is defined as the ratio between the sensible and latent heat fluxes. It was calculated for both simulation and observations at 3 points over the Amazon as in da Rocha et al. (2012); initially we determined the average of the latent and sensible heat fluxes for the 3 experimental sites, and then β. The observations are from the micrometeorological measurements at experimental sites over the Amazon rainforest: Manaus KM34 (2.6090° S, 60.2093° W), Santarem KM67 (2.8853° S, 54.9205° W) and Santarem KM83 (3.0502° S, 54.9280° W). A summary of these micrometeorological observations can be obtained in Negrón Juárez et al. (2007) and Rocha et al. (2009). First, we calculated the average of the latent and sensible heat fluxes for the 3 experimental sites, and then β.

3. RESULTS

Before discussing the sensitivity experiments (see Table 1), we will describe the precipitation and air temperature seasonal averages (1990–1999) for the austral summer (DJF) and winter (JJA) from CRU/CMAP and S_CTRL. During summer, a northwest–southeast precipitation band with ~8 mm d^{-1}, from the Amazon to southeastern Brazil, indicates the continental part of the SACZ in CRU/CMAP (Fig. 2a). Similar precipitation values occur in the Atlantic portion of the ITCZ located between the equator and 5° N at this time of year. In many aspects, S_CTRL (Fig. 2c) resembles CMAP (Fig. 2a), but there are differences in the precipitation amounts in some regions. S_CTRL (Fig. 2e) overestimates the precipitation over northwestern Argentina, central-western Brazil, Bolivia, southern Peru and in extreme northern SA. On the other hand, it underestimates rainfall in the ITCZ, the oceanic branch of the SACZ, the Amazon and in a small part of southeastern SA. During winter (Fig. 2b), the continental maximum of precipitation in CMAP occurs over northwestern SA

(8 to 12 mm d^{-1}); a secondary maximum is also found over southeastern SA (4 to 8 mm d^{-1}). In this season, weak precipitation occurs over Argentina and central and northeastern Brazil. In this last region precipitation is associated with the displacement of the Atlantic ITCZ to the Northern Hemisphere. Regarding the spatial pattern of precipitation, S_CTRL agrees better with CMAP in winter (Fig. 2d) than in summer (Fig. 2c). Moreover, over the continent there are fewer regions with precipitation bias during winter (Fig. 2f). Among these, the ITCZ, northeastern coastal Brazil and from southeastern SA to the southwestern South Atlantic Ocean have negative bias. In this last area, the deficit of precipitation is a common problem of many RCMs (Solman et al. 2013) and also of RegCM3 (da Rocha et al. 2012). For S_CTRL, positive bias is found in extreme northern SA and from central Chile to southern Bolivia (Fig. 2f).

The observed air temperature in summer is higher (>26°C) over the north, northeast and west sectors of the continent and lower over mountainous regions, such as the Andes (<16°C) and southeastern Brazil (16 to 20°C), and in latitudes poleward of 40° S (Fig. 3a). During winter, there is a general advance of cold air northwards, with temperature values of 16°C reaching lower latitudes (20° S) than in summer (Fig. 3a). In both summer and winter, S_CTRL underestimates the observed air temperature by about 2 to 4°C in almost all of SA (Figs. 3e,f). The few areas of overestimation (2 to 4°C) occur over eastern Argentina in summer (Fig. 3e) and central-southern Amazon in winter (Fig. 3f). In summer the dry bias in precipitation over the Amazon (Fig. 2e) in S_CTRL is not associated with a warm bias in air temperature (Fig. 3e); on the contrary, there is cold bias. As in previous versions of RegCM, the cold bias in air temperature in S_CTRL can be associated with the Grell convective scheme. As discussed in Giorgi et al. (2004) and Martínez-Castro et al. (2006), this scheme is very efficient in the vertical redistribution of heat and moisture, which results in cold/dry (warm/moist) conditions in the low (middle) troposphere.

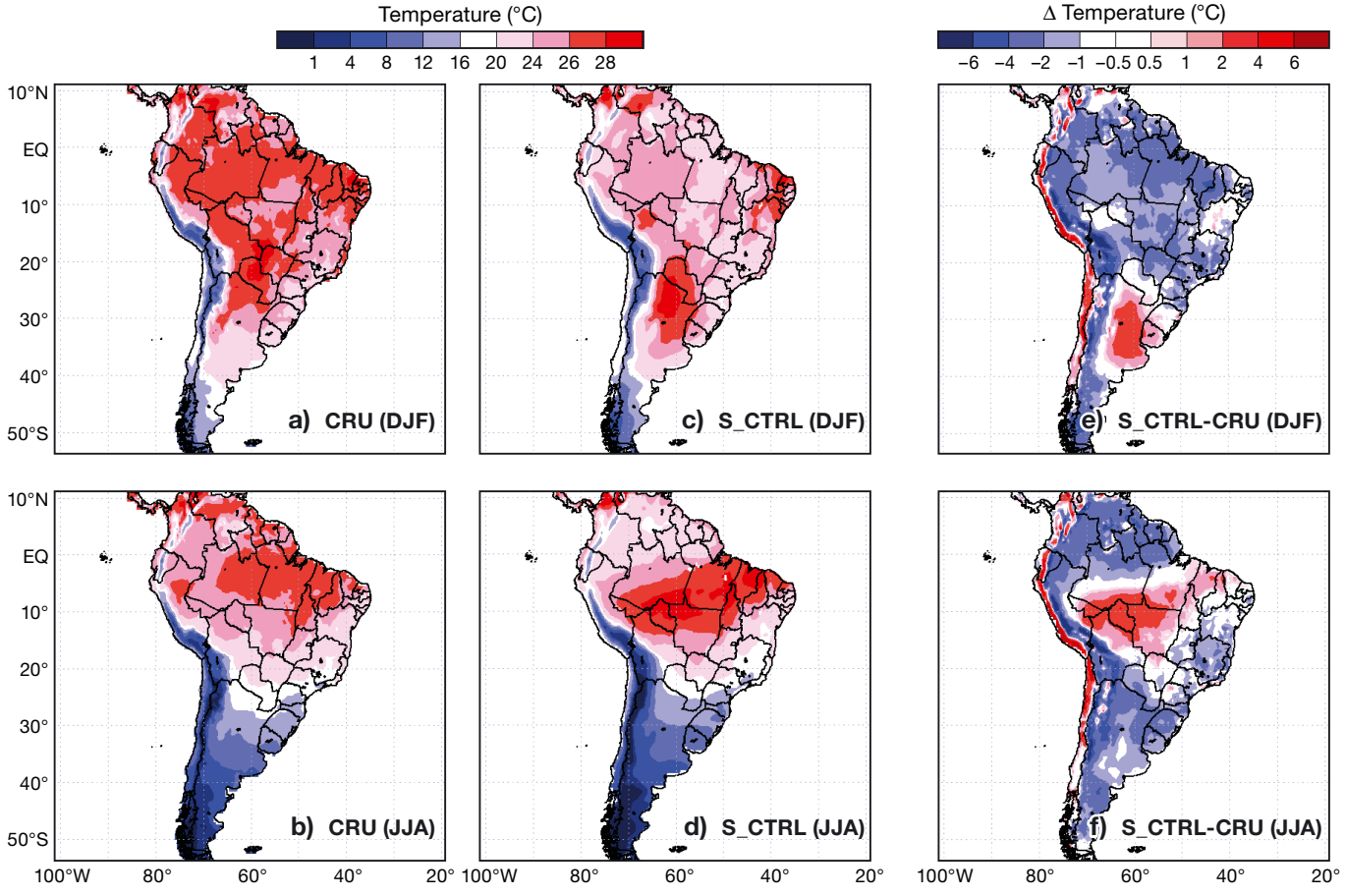

Fig. 3. Air temperature average (1990–1999) in (a,b) DJF and (d,e) JJA from CRU and S_CTRL, and (c,f) difference between datasets (S_CTRL-CRU) in each season

3.1. Sensitivity to the convective schemes: S_CTRL, S_MIT and S_Tiedtke

This section compares the performance of 3 of the convective schemes presented in Table 1 (Mixed1: S_CTRL, Tiedtke: S_Tiedtke, and MIT: S_MIT) in the simulation of the climatology of precipitation and air temperature over SA. During austral summer (DJF), S_CTRL overestimates the precipitation over northern-central SA, while negative rainfall biases occur over southern Amazon, ITCZ and the oceanic branch of the SACZ (Fig. 2e). On the other hand, a different spatial pattern of precipitation bias is shown by the S_MIT experiment (Fig. 4b). The use of the MIT convective scheme results in very wet conditions over almost all of Brazil, Bolivia, Peru, Ecuador, and western Argentina. In this experiment, the dry biases occur over southeastern SA, eastern Colombia, the extreme north of SA (Guyana and Suriname) and in the tropical Atlantic ITCZ. This dry condition over the ITCZ intensifies and extends southward covering a large part of north-northeastern SA in the S_Tiedtke experiment (Fig. 4a). This simulation also increases the region having negative precipitation biases in southeastern SA as compared to S_CTRL and S_MIT. A west–east band (from Peru, Bolivia, and crossing from central-western to southeastern Brazil) of positive rainfall biases is also present in the S_Tiedtke (Fig. 4a). The spatial pattern of precipitation biases in S_MIT and S_Tiedtke may — at least in part — be associated with the differences in evapotranspiration. In a large part of the areas where S_MIT is wetter than CMAP (Fig. 4b) there is also a larger evapotranspiration rate than S_CTRL (Fig. 5b). For the whole continental SA we obtain an annual mean evapotranspiration rate of 2.88 and 3.61 mm d^{-1}, respectively, in S_CTRL and S_MIT. We attempt to understand this feature by calculating for the annual mean the spatial pattern correlation between the differences (S_MIT minus S_CTRL) of evapotranspiration and of some near surface variables only over the continent. The larger evapotranspiration in S_MIT occurs mainly due to the greater water content in the soil layers (upper layer plus root zone) in S_MIT than in S_CTRL. The correlation is high and positive (+0.86) indicating that in regions with greater (smaller) soil water content the evapotranspiration is higher (lower).

In S_Tiedtke the areas with large underestimation of rainfall (over northern and southeastern SA in Fig. 4a) are the same areas with evapotranspiration rate smaller than in S_CTRL (Fig. 5a). Also in this case, there is a high positive spatial pattern correlation (0.93) between the differences (S_Tiedtke minus S_CTRL) of soil moisture and of evapotranspiration, justifying the decrease (increase) of evapotranspiration in the areas with lower (higher) total soil water content. In addition, in the wetter (S_MIT) and dryer (S_Tiedtke) simulations there is a different partition of the total rainfall between convective and grid scale. In S_MIT the large evapotranspiration leads to an increase in moist static energy, contributing to the activation of the convective scheme. Consequently, 91% of the total precipitation is convective. The opposite occurs in S_Tiedtke where the lower evapotranspiration reduces both the moist static energy and the fraction of the convective rainfall to 61% of the total rainfall.

The precipitation biases for the sensitivity experiments in austral winter (JJA) are shown in Fig. 6. In this season, over continental SA a reduction of the areas presenting precipitation bias is seen in both S_CTRL (Fig. 2f) and S_MIT (Fig. 6b) as compared to summer. However, both experiments simulate a band of positive rainfall biases in the southern domain. Fig. 6a shows that even in winter S_Tiedtke continues to present large areas with precipitation underestimation over the continental SA (most of northern SA, North Atlantic ITCZ, southwestern South Atlantic Ocean and the eastern part of northeastern of Brazil), making it the poorer convective scheme in winter. The only region where S_Tiedtke simulates smaller biases than S_CTRL and S_MIT is in the oceanic areas at higher latitudes (Figs. 2f and 6a,b).

Figs. 7 and 8 present the air temperature biases during austral summer and winter, respectively. In summer, the large positive differences of S_MIT in relation to CRU occur over northwestern SA and central-northern Argentina, while negative differences are noticed over southeastern Brazil, southern Argentina and the Andes Mountains (Figs. 7b). The air temperature bias in S_Tiedtke (Fig. 7a) presents a spatial pattern similar to that of S_MIT (Fig. 7b). However, in S_Tiedtke the more intense warm bias covers practically all of northern-northeastern SA. In S_Tiedtke the warm biases can be due to the underestimation of precipitation and to greater sensible heat flux transfer from surface to the low troposphere than S_CTRL (Fig. not shown). On the other hand, S_CTRL (Fig. 3e) has a cold bias over most of SA, even in areas where a precipitation deficit occurs (Fig. 2e). A common feature in the 3 simulations with different convective schemes (S_CTRL, S_MIT and S_Tiedtke) is the warm bias over southeastern SA, which could be a result of both precipitation under-

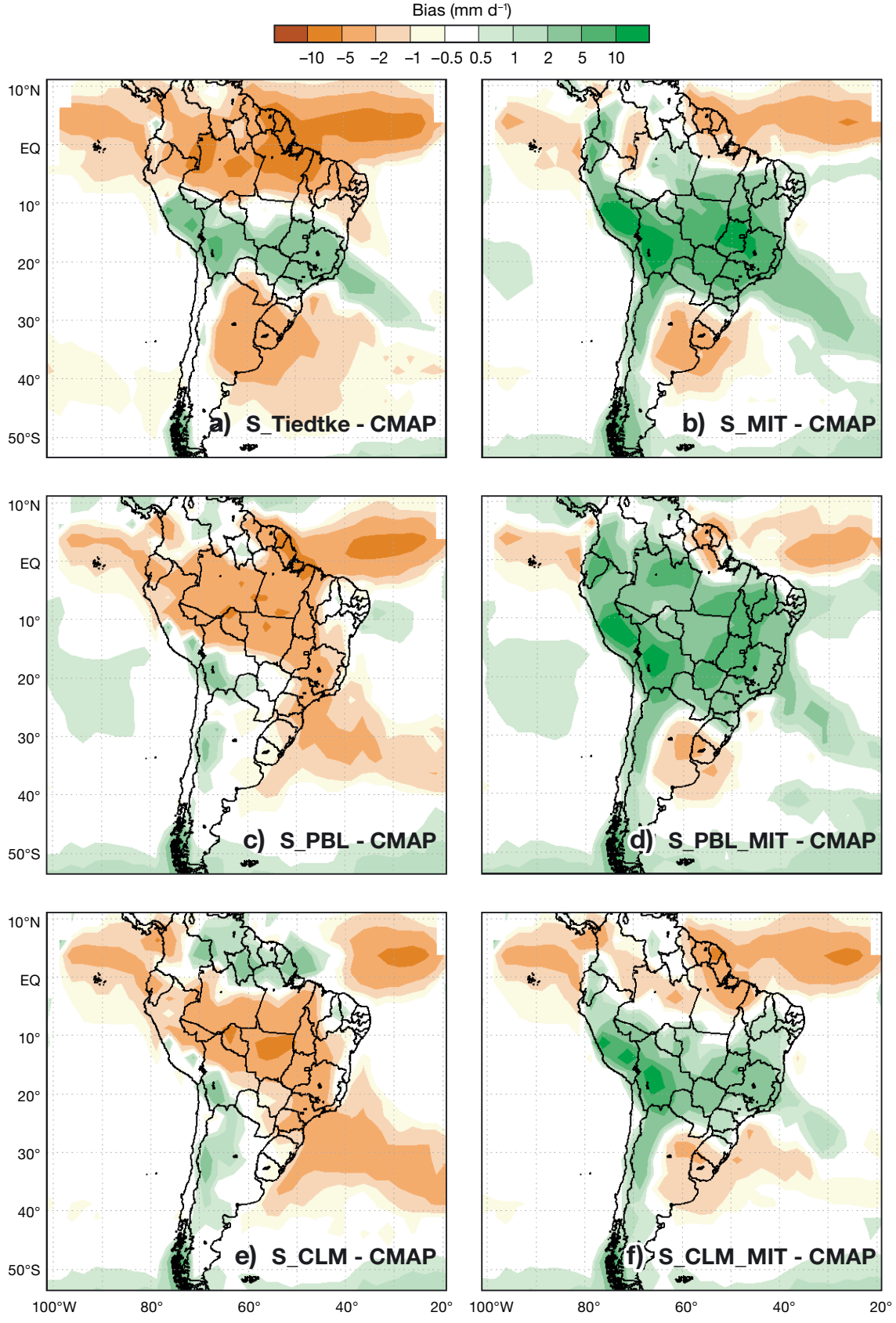

Fig. 4. DJF precipitation bias relative to CMAP in (a) S_Tiedtke, (b) S_MIT, (c) S_PBL, (d) S_PBL_MIT, (e) S_CLM, and (f) S_CLM_MIT

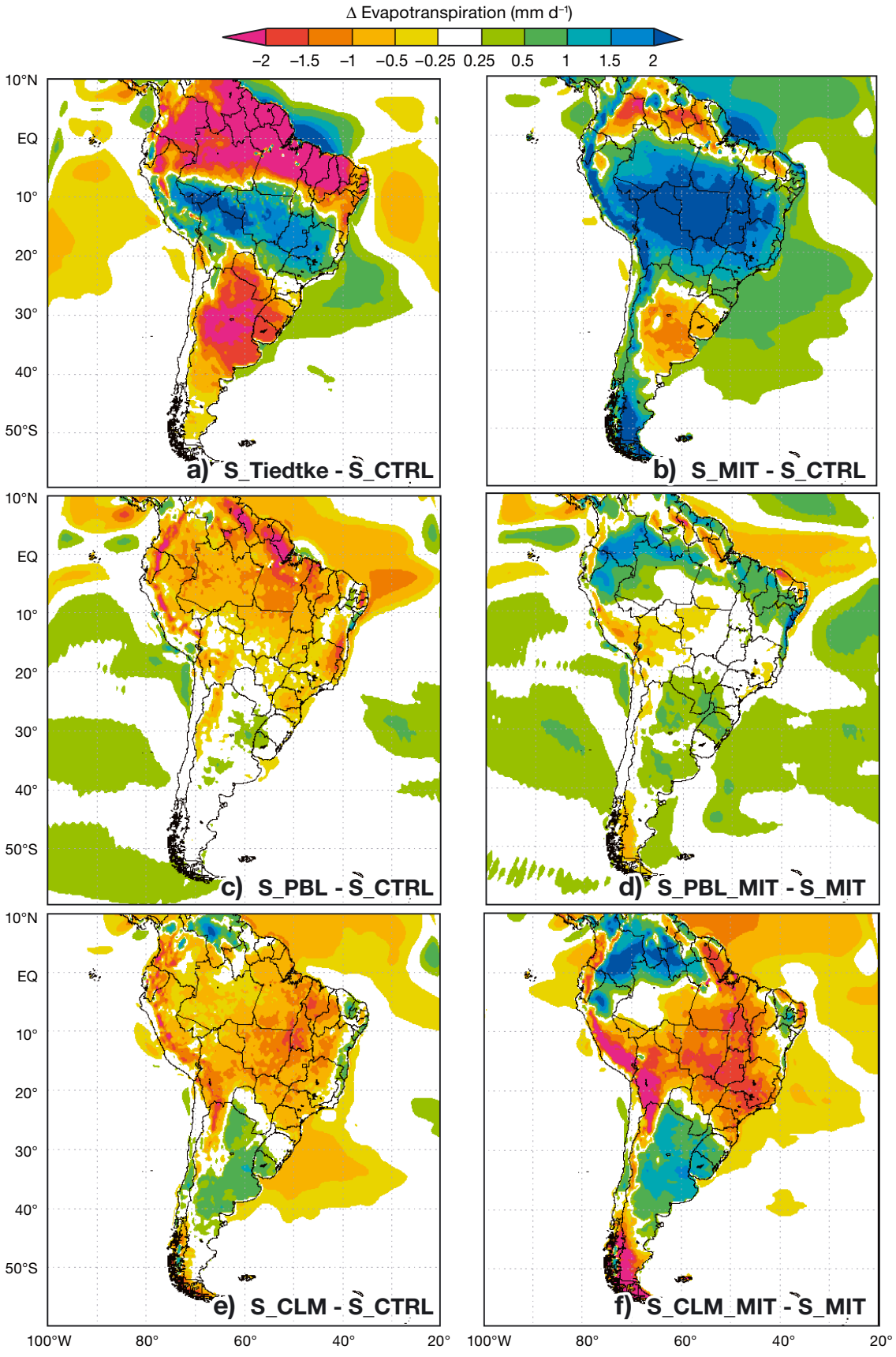

Fig. 5. DJF evapotranspiration differences in: (a) S_TIEDTKE – S_CTRL, (b) S_MIT – S_CTRL, (c) S_PBL – S_CTRL, (d) S_PBL_MIT – S_MIT, (e) S_CLM – S_CTRL and (f) S_CLM_MIT – S_MIT

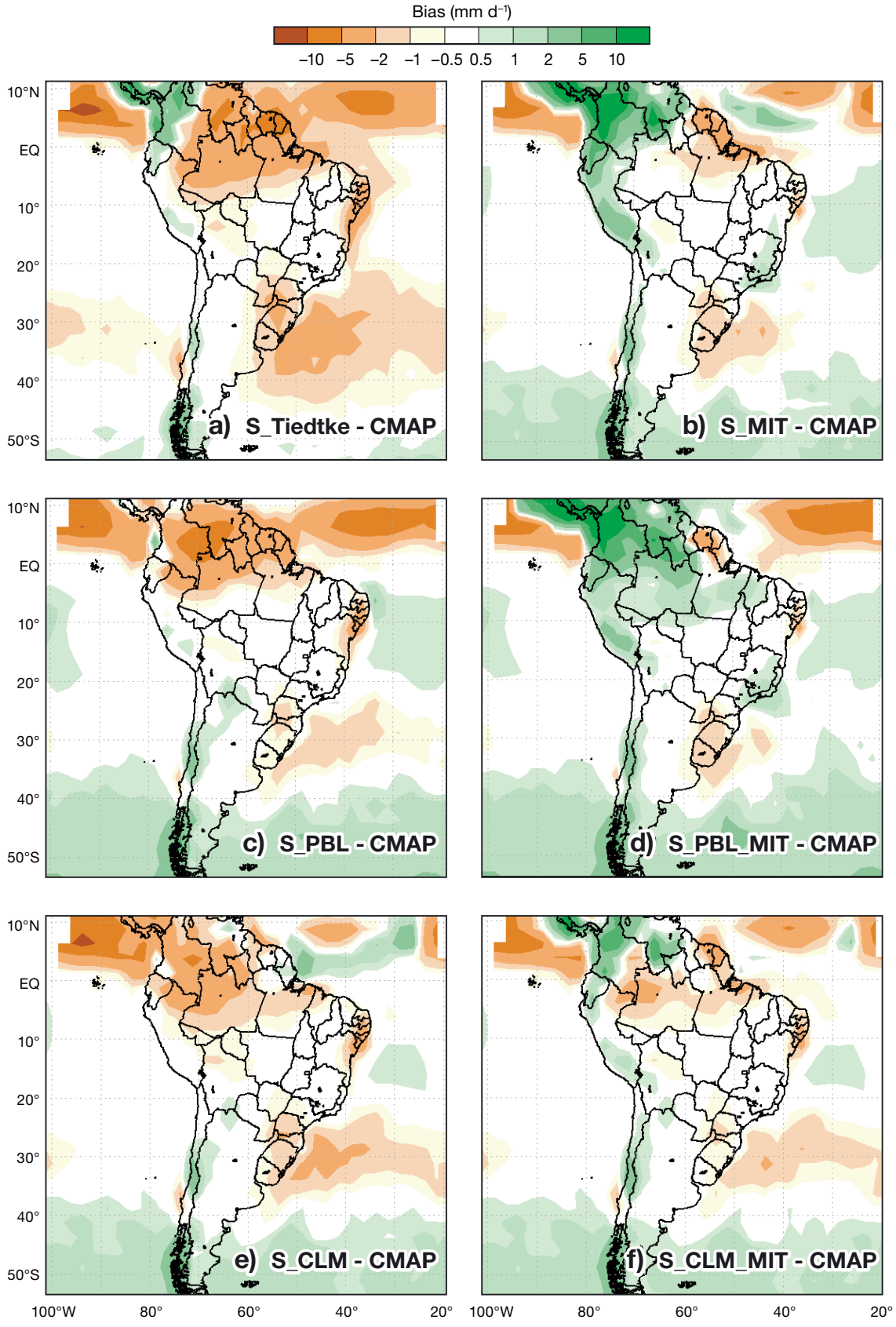

Fig. 6. Similar to Fig. 4 but for JJA precipitation bias

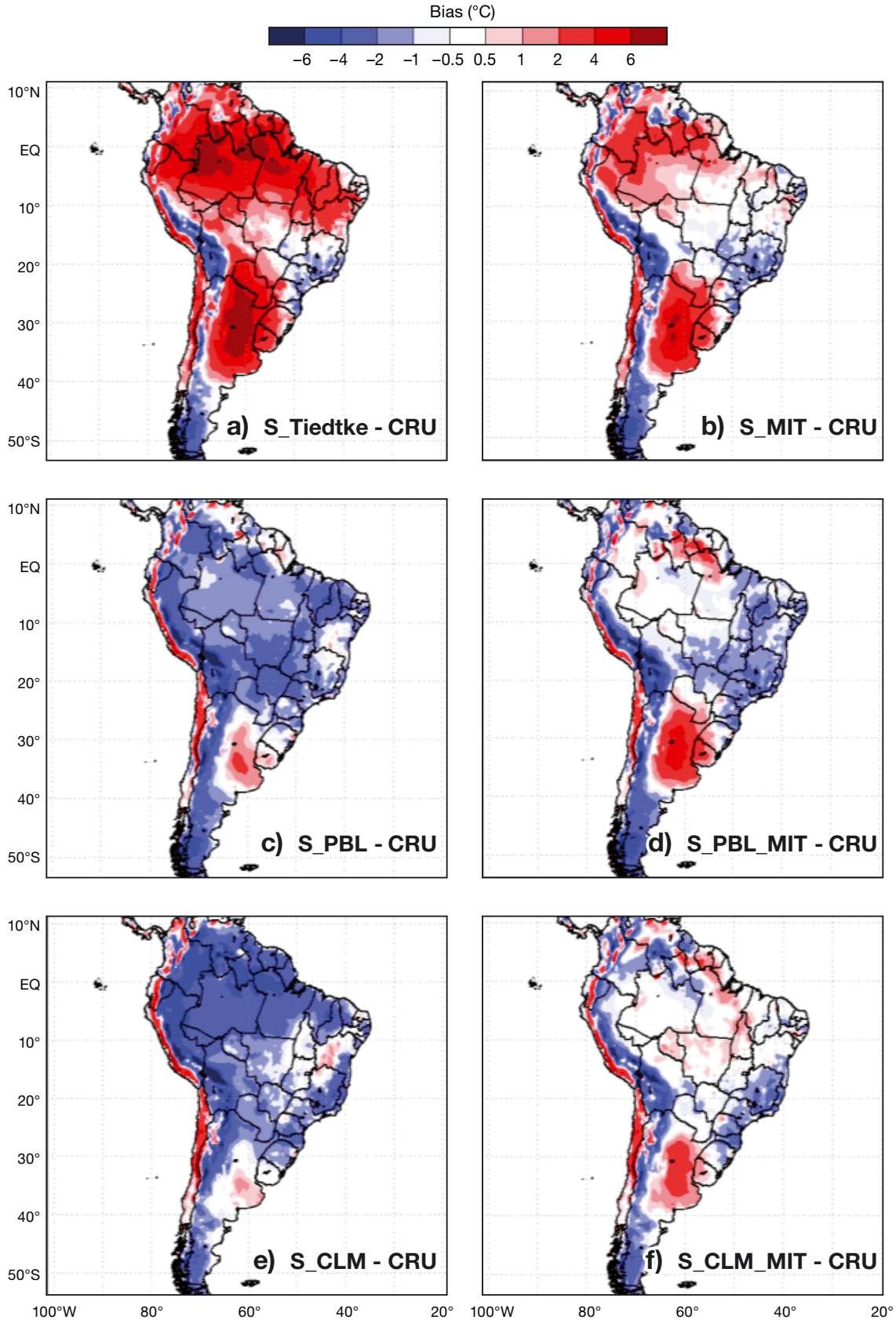

Fig. 7. DJF air temperature bias relative to CRU in (a) S_Tiedtke, (b) S_MIT, (c) S_PBL, (d) S_PBL_MIT, (e) S_CLM, and (f) S_CLM_MIT

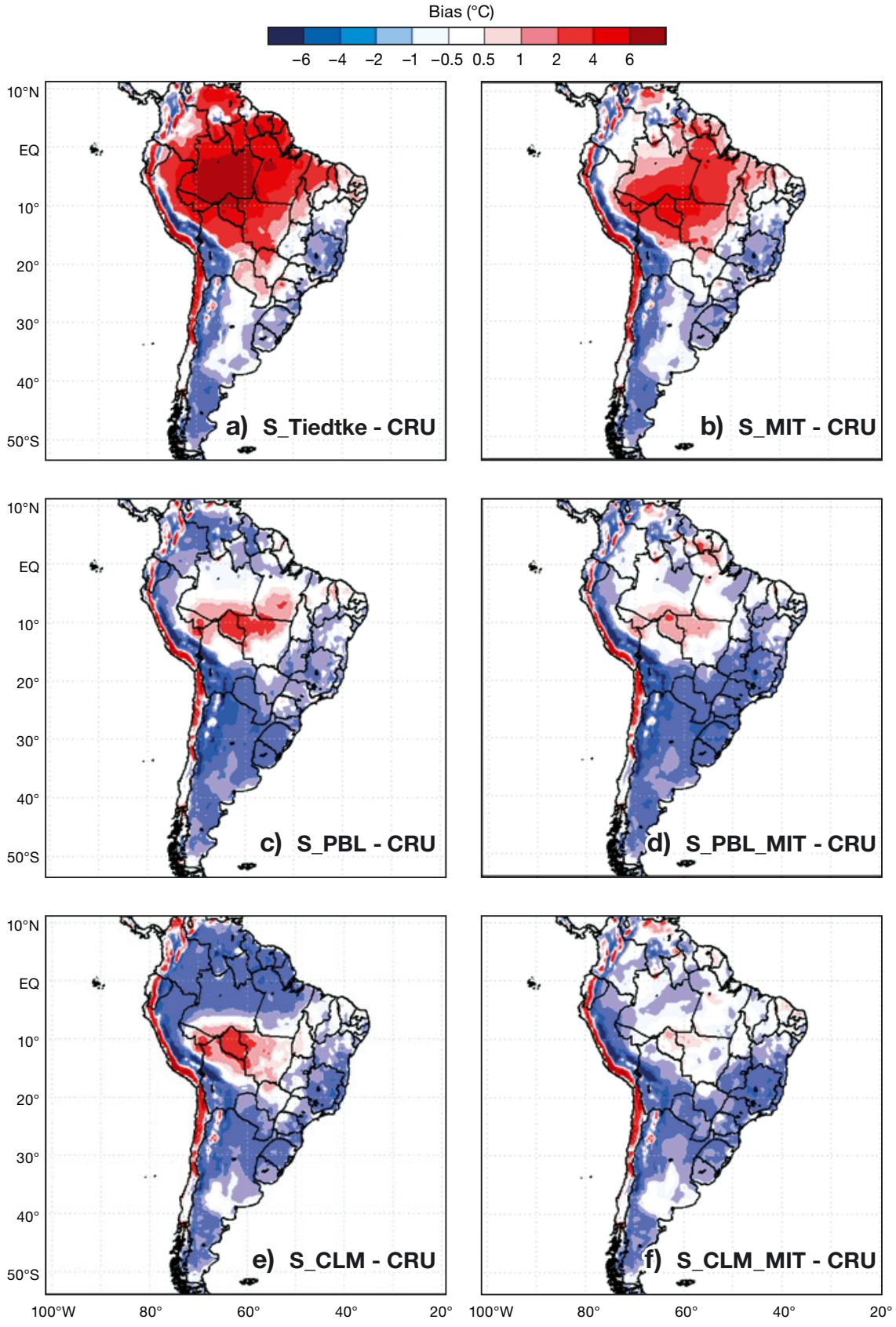

Fig. 8. Similar to Fig. 7 but for JJA air temperature bias (°C)

estimation (Figs. 2e and 4a,b) and the PBL scheme (see Section 3.2).

In winter, S_CTRL simulates a warm bias over the southern Amazon and the Andes Mountains and as in summer, a cold bias is seen in the other sectors of SA (Fig. 3f). On other hand, in S_Tiedtke (Fig. 8a) and S_MIT (Fig. 8b) the air temperature simulation errors have a different spatial pattern. In these experiments there are warm biases over the Amazon and vicinity and cold biases over eastern Brazil and extreme southern Argentina.

3.2. Sensitivity to the PBL schemes: S_CTRL, S_PBL and S_PBL_MIT

In this section we discuss the impact of 2 different PBL schemes, Holtslag (S_CTRL) and UW-PBL (S_PBL), upon the simulated climatology. In addition, we investigate whether the association of the MIT scheme with UW-PBL (S_PBL_MIT) might reduce the excessive positive precipitation bias of the S_MIT experiment during austral summer (Fig. 4b).

Comparing the S_CTRL (Fig. 2e) and S_PBL (Fig. 4c) precipitation biases we can see that in summer over the SACZ (continental and oceanic branches) and ITCZ regions the UW-PBL scheme contributes to drier conditions in S_PBL than Holtslag in S_CTRL. A large underestimation of rainfall is also simulated during winter over northwestern SA and the ITCZ, due to the influence of the UW-PBL scheme (Fig. 6c). The increase of dry bias in S_PBL is mainly related to the reduction in the evapotranspiration rate compared with S_CTRL (Fig. 5c). Considering the continental SA, the annual mean evapotranspiration rates are 2.35 and 2.88 mm d^{-1}, respectively, in S_PBL and S_CTRL. For lower evapotranspiration in S_PBL, the differences (S_PBL minus S_CTRL) of soil moisture and of evapotranspiration also present a high positive spatial pattern correlation (+0.85). As the correlation is positive we may interpret that the areas with less (more) soil water content are also regions with less (more) evapotranspiration in S_PBL compared with S_CTRL. A second feature is the increase of surface drag stress in the same areas with less evapotranspiration, which is explained by spatial pattern correlation of −0.77 between the differences (S_PBL minus S_CTRL) in evapotranspiration and in surface drag stress. Compared with S_CTRL, in the S_PBL the lowering of the PBL height is not directly related to the increase of evapotranspiration, since the differences (S_PBL minus S_CTRL) present weak spatial correlation of only −0.21. In general, regions with dry bias in S_PBL (Figs. 4c and 6c) become wet when the MIT scheme is used together with UW-PBL scheme (Figs. 4d and 6d). This last combination of parameterizations (S_PBL_MIT) contributes to increasing the evapotranspiration in some parts of SA compared with the S_MIT (Fig. 5d) and S_PBL (Fig. not shown) and consequently yield more precipitation. In S_MIT_PBL the regions with greater (less) evapotranspiration are also positively (negatively) correlated with regions with more (less) soil water content (correlation of 0.84) and surface drag stress (correlation −0.80). However, in the S_MIT_PBL, the negative correlation between regions with lower (higher) PBL height and higher (lower) evapotranspiration is greater (−0.64) than for S_PBL (−0.21). This could permit the development of clouds with lower base in S_MIT_PBL than in S_PBL, explaining at least in part the large amount of precipitation in S_MIT_PBL. In this experiment the large part (87%) of total rainfall results from the convection schemes; this result was also obtained for S_MIT (91%).

For the air temperature, in both summer and winter, compared to CRU the configuration S_PBL (Figs. 7c and 8c) produces a cold bias over almost all of SA, even in the regions with large precipitation underestimation. In general, the values and spatial pattern of the temperature biases from S_PBL resemble that of S_CTRL (Figs. 3e,f), suggesting that the Grell convective scheme dominates over the UW-PBL scheme to produce the cold bias. When S_MIT (Figs. 7b and 8b) and S_PBL_MIT (Figs. 7d and 8d) simulations are compared, the UW-PBL scheme contributes to the reduction of the warm bias of the Holtslag scheme (S_MIT) over northwestern and southeastern SA. In this last area, independent of convective scheme, UW-PBL reduces the excessive warm bias of Holtslag in summer by means of decreasing the sensible heat fluxes (Figs. not shown). Güttler et al. (2013) used the RegCM4.2 (with BATS and MIT schemes) to evaluate the sensitivity to the Holtslag and UW-PBL schemes over Europe. In this analysis they also obtained a reduction of the warm bias with UW-PBL. These authors also suggest that the smaller entrainment of potentially warm free tropospheric air into the boundary layer in UW-PBL can contribute to decreasing the warm bias.

3.3. Sensitivity to the surface schemes: S_CTRL, S_CLM and S_CLM_MIT

As shown in Table 1, we analyzed the influence of land surface schemes by changing the BATS to the

CLM in the S_CLM experiment. Besides this, we carried out another simulation using the MIT convective scheme together with the CLM (S_CLM_MIT).

In the austral summer, by comparing S_CLM with CMAP (Fig. 4e) we can see the underestimation of precipitation over the SACZ (continental and oceanic branches) and ITCZ regions. The spatial pattern of this bias differs from that of S_CTRL (which uses the BATS scheme), which has a smaller dry bias in these oceanic regions and the continent (over southern Amazon, Fig. 2e). On the other hand, the coupling of CLM with the MIT scheme (Fig. 4f) reduces the significant overestimate of precipitation in tropical and subtropical SA (from 5° S to 25° S) and also reduces the dry bias over southeastern SA present in S_MIT (Fig. 4b). For winter, S_CLM (Fig. 6e) simulates more areas with negative precipitation bias (northwestern SA, southern Brazil and the adjacent South Atlantic Ocean) than S_CTRL (Fig. 2f). In addition, during winter S_CLM_MIT (Fig. 6f) presents smaller precipitation biases than S_MIT (Fig. 6b). This occurs for the positive and negative rainfall biases, respectively, over northwestern SA and southern Brazil. Therefore, in both summer and winter, the combination of CLM with the MIT scheme (S_CLM_MIT) contributes to a decrease in wet bias when the combination of the BATS and MIT schemes is used. This improvement in the precipitation simulated by S_CLM_MIT is associated with CLM, which contributes to the reduction in the excessive evapotranspiration rate simulated by S_MIT (Fig. 5b,f). This fact was also documented by Steiner et al. (2009) and Diro et al. (2012). According to Steiner et al. (2009), soil moisture at the surface is underestimated by CLM compared to BATS, and since the evaporation from bare soil is the main contributor to evapotranspiration in CLM it decreases the latent heat fluxes and precipitation. As a result of the drier soil layers and reduced latent heating, sensible heat fluxes are generally higher in CLM.

The coupling of CLM and the MIT scheme in S_CLM_MIT also helps to reduce the temperature errors over a large part of SA during the summer (Fig. 7f). The warm biases over northwestern and southeastern SA are smaller in S_CLM_MIT than in S_MIT (Fig. 7b). Moreover, S_CLM_MIT presents a strong improvement in the simulated air temperature compared to S_CTRL (Fig. 3e) and S_CLM (Fig. 7e), which simulate a cold bias over a large part of SA. Although S_CLM_MIT overestimates the precipitation over central-western SA (Fig. 4f), it does not produce a cold bias. This fact can be associated in part with the influence of the convective scheme. In S_CTRL (Fig. 3e) and S_CLM (Fig. 7e), which use the Grell scheme over the continent, the underestimation of air temperature is a common feature in both. As discussed, the Grell convective scheme is very efficient in the vertical redistribution of heat and moisture, explaining in part its near-surface cold bias (Giorgi et al. 2004, Martínez-Castro et al. 2006). Considering all simulations in this study (Fig. 7), the smallest warm bias over northeastern Argentina is simulated by S_CLM (Fig. 7e).

In winter, S_CTRL (Fig. 3f) and S_CLM (Fig. 8e) show a similar spatial pattern in the bias, i.e. they are warmer than CRU over the southern Amazon and colder in other areas. As in summer, the temperature bias over Amazon is smaller in S_CLM_MIT (Fig. 8f) than in the other simulations. Overall, considering all simulations and all SA, the air temperature in winter is slightly better simulated by S_CLM_MIT. The next section shows that there is a better surface energy partitioning in S_CLM_MIT, which contributes to the improvement of the simulated air temperature.

3.4. Annual cycle: precipitation and air temperature

The analyses of Sections 3.1, 3.2 and 3.3 suggest that for the whole of SA the configurations of S_CTRL and S_CLM_MIT are better for the simulation of the precipitation and air temperature, respectively. However, sometimes these configurations may not be appropriate to the specific regions. Thus, we evaluated the performance of the simulations over 5 continental subdomains (indicated in Fig. 1) over the annual cycle by means of statistical indices (bias, SD and Pearson correlation coefficient) applied to the DJF and JJA seasons. The SD was used as a measure of the interannual variability, with high (low) values indicating greater (weaker) interannual variability.

In Fig. 9a, CMAP shows the wet season in the Amazon subdomain (AMZ) occurring from October to March and is associated with the SAM (Vera et al. 2006, Marengo et al. 2012), while the dry season lasts from April to September. In general, the phase of the annual cycle of precipitation is simulated by all experiments. However, in terms of intensity, S_CTRL presents smaller biases for precipitation from June to November and S_CLM_MIT from December to March (Fig. 9a). Since DJF is the peak of the AMZ rainy season, we will discuss the statistical analysis for this season.

In DJF, compared with CMAP (Fig. 9a) the MIT scheme (S_PBL_MIT and S_MIT) tends to produces

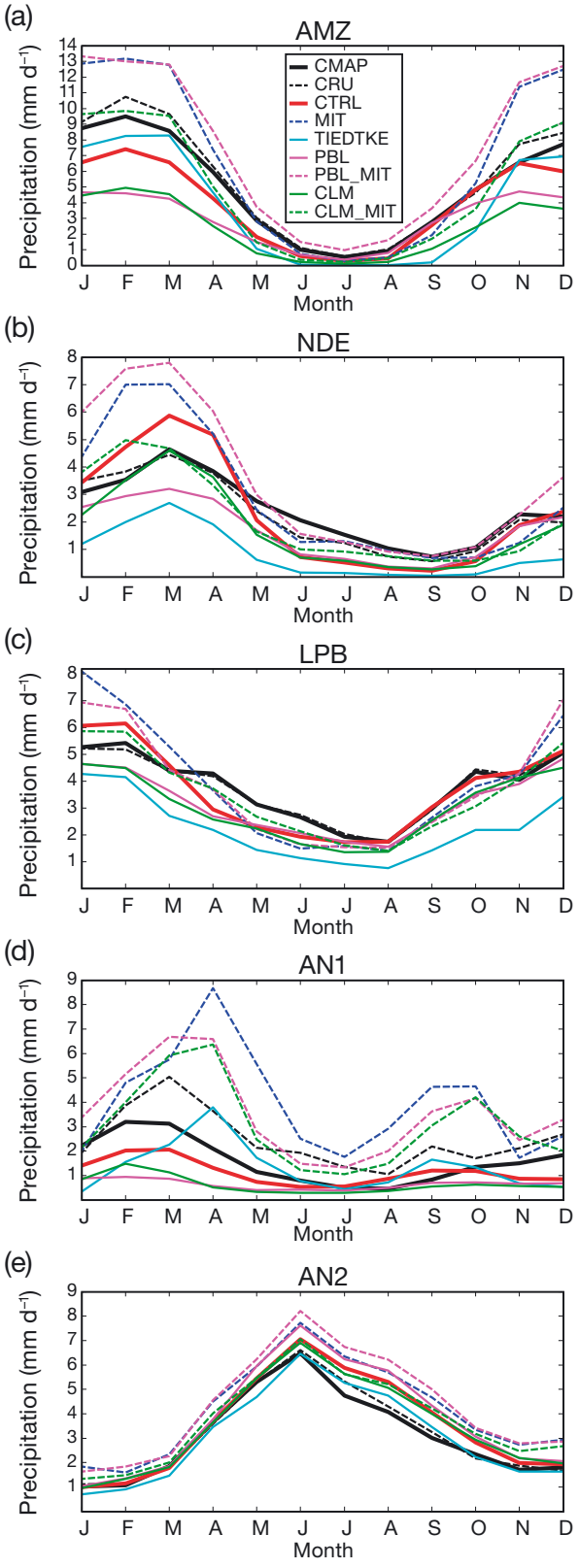

AMZ	MEAN	SD	BIAS	r
CMAP	8.6 (0.8)	1.4 (0.5)	–	–
CRU	9.4 (0.9)	1.5 (0.4)	0.8 (0.1)	0.6 (0.7)
S_CTRL	6.6 (0.4)	1.2 (0.3)	–2.0 (–0.4)	0.6 (0.6)
S_MIT	12.8 (0.5)	2.6 (0.4)	4.2 (–0.3)	0.5 (0.4)
S_TIEDTKE	7.6 (0.0)	1.6 (0.0)	–1.0 (–0.8)	0.7 (0.3)
S_PBL	4.5 (0.6)	0.4 (0.3)	–4.1 (–0.2)	0.6 (0.6)
S_PBL_MIT	13.0 (1.3)	1.5 (0.5)	4.4 (0.5)	0.4 (0.6)
S_CLM	4.3 (0.2)	1.0 (0.1)	–4.3 (–0.6)	0.7 (0.7)
S_CLM_MIT	9.5 (0.3)	1.5 (0.2)	0.9 (–0.5)	0.5 (0.6)

NDE	MEAN	SD	BIAS	r
CMAP	2.9 (1.5)	1.2 (0.7)	–	–
CRU	3.1 (1.1)	1.2 (0.5)	0.2 (–0.4)	0.9 (0.9)
S_CTRL	3.5 (0.5)	1.3 (0.3)	0.6 (–1.0)	0.6 (0.8)
S_MIT	4.6 (1.2)	2.6(0.4)	1.7 (–0.3)	0.5 (0.7)
S_TIEDTKE	1.3 (0.1)	1.1(0.1)	–1.6 (–1.4)	0.4 (0.6)
S_PBL	2.5 (0.6)	0.5 (0.3)	–0.4 (–0.9)	0.5 (0.8)
S_PBL_MIT	5.7 (1.2)	2.2 (0.5)	2.8 (–0.3)	0.4 (0.8)
S_CLM	2.6 (0.5)	1.0 (0.2)	–0.3 (–1.0)	0.5 (0.8)
S_CLM_MIT	3.6 (0.9)	1.8 (0.2)	0.7 (–0.6)	0.4(0.8)

LPB	MEAN	SD	BIAS	r
CMAP	5.2 (2.1)	1.1 (0.9)	–	–
CRU	5.2 (2.2)	0.9 (0.8)	–0.0 (0.1)	0.9 (0.9)
S_CTRL	5.8 (1.8)	1.4 (0.7)	0.6 (–0.3)	0.7 (0.6)
S_MIT	7.1 (1.5)	2.0 (0.5)	1.9 (–0.6)	0.3 (0.5)
S_TIEDTKE	3.9 (0.9)	1.5 (0.5)	–1.3 (–1.2)	0.3 (0.5)
S_PBL	4.7 (1.8)	0.9 (0.6)	–0.5 (–0.3)	0.5 (0.6)
S_PBL_MIT	6.9 (1.6)	1.4 (0.5)	1.7 (–0.5)	0.2 (0.5)
S_CLM	4.5 (1.4)	1.0 (0.6)	–0.7 (–0.7)	0.5 (0.7)
S_CLM_MIT	5.7 (1.7)	1.3 (0.6)	0.5(–0.4)	0.6 (0.5)

AN1	MEAN	SD	BIAS	r
CMAP	2.4 (0.6)	1.9 (0.2)	–	–
CRU	2.8 (1.4)	2.2 (0.6)	0.4 (0.8)	0.2 (0.6)
S_CTRL	1.4 (0.6)	0.7 (0.2)	–1.0 (0.0)	0.7 (-0.3)
S_MIT	3.1 (2.4)	2.2 (0.7)	0.7 (1.8)	0.3 (0.3)
S_TIEDTKE	0.8 (0.6)	0.8 (0.3)	–1.6 (0.0)	0.5 (0.6)
S_PBL	0.8 (0.4)	0.3 (0.1)	–1.6 (–0.2)	0.8 (0.0)
S_PBL_MIT	3.9 (1.6)	2.1 (0.4)	1.5 (1.0)	0.7 (0.0)
S_CLM	0.9 (0.3)	0.6 (0.1)	–1.5 (–0.3)	0.6 (0.0)
S_CLM_MIT	2.7 (1.2)	1.5 (0.3)	0.3 (0.6)	0.6 (0.3)

AN2	MEAN	SD	BIAS	r
CMAP	1.3 (5.1)	0.8 (2.0)	–	–
CRU	1.3 (5.4)	0.7 (2.0)	0.0 (0.3)	0.9 (0.9)
S_CTRL	1.4 (6.1)	1.0 (2.1)	0.1 (1.0)	0.9 (0.8)
S_MIT	2.1 (6.6)	1.6 (2.3)	0.8 (1.5)	0.7 (0.8)
S_TIEDTKE	1.1 (5.5)	0.9 (1.9)	–0.2 (0.4)	0.9 (0.8)
S_PBL	1.5 (6.5)	1.1 (2.2)	0.2 (1.4)	0.8 (0.8)
S_PBL_MIT	2.1 (7.0)	1.6 (2.3)	0.8 (1.9)	0.8 (0.9)
S_CLM	1.4 (5.9)	1.0 (2.1)	0.1 (0.8)	0.8 (0.8)
S_CLM_MIT	1.8 (5.8)	1.4 (2.1)	0.5 (0.7)	0.8 (0.9)

Fig. 9. Annual cycle of precipitation (left column) obtained from simulations and analyses in the 5 subdomains, and statistics (right column): mean, standard deviation (SD), bias and Pearson correlation coefficient (r) during DJF and JJA. Parentheses: JJA values

higher positive rainfall biases in AMZ, except when associated with the CLM scheme (S_CLM_MIT). The large underestimates of precipitation occur in the S_PBL and S_CLM experiments. In terms of the SD (Fig. 9), overall the simulated values are near those of CMAP and CRU, except for S_MIT and S_PBL. Compared with CMAP/CRU, higher (lower) than observed interannual variability of precipitation is simulated by S_MIT (S_PBL). Considering all experiments, S_CLM_MIT and S_PBL_MIT have values close to the CMAP/CRU, i.e. show considerable ability in simulating the observed interannual variability of rainfall.

The lowest biases in the air temperature in DJF over AMZ occur in S_MIT, S_PBL_MIT, and S_CLM_MIT (Fig. 10a). In addition, compared with CRU, the S_CLM_MIT reproduces both the phase and values of the annual cycle of air temperature over AMZ (Fig. 10a). Most experiments, except S_PBL_MIT and S_CLM_MIT, overestimate the interannual variability of the air temperature in DJF (Fig. 10a). In summary, for AMZ the air temperature throughout the year is closer to observation in S_CLM_MIT. Moreover, this experiment also performs well in the representation of the precipitation, mainly at the peak of the rainy season.

The better performance of S_CLM_MIT over AMZ is discussed through an analysis of the Bowen ratio (β), which is helpful in understanding the energy partition. In addition, we also analyze this feature in S_CTRL and S_MIT (Fig. 11). The observed β is practically constant throughout the year. However, in the S_MIT β is nearly constant from November to May and reaches values higher than one from July to September. Values of $\beta > 1$ mean that a major amount of available energy is being used for heating the air, with less energy is available for the evapotranspiration process. Indeed, Fig. 10a shows higher air temperatures in this period in S_MIT compared with S_CTRL and S_CLM_MIT. During winter, S_CTRL also overestimates β, while S_CLM_MIT presents values more similar to the observations. This indicates an improvement of the surface energy partitioning in S_CLM_MIT, with consequent good agreement with observations for the simulated precipitation (Figs. 4f and 6f) and air temperature (Figs. 7f and 8f) over the Amazon region.

As shown by CMAP, the rainy season in northeastern Brazil (NDE) extends from January to May with a peak in March (Fig. 9b), and is mainly controlled by the meridional displacement of the ITCZ (Hastenrath & Heller 1977 Hastenrath 1991). Fig. 9b indicates that the simulations capture the pattern of the observed annual cycle of the precipitation. However, most of the experiments have positive precipitation biases during rainy season, while there is a general underestimation of rainfall from May to November (Fig. 9b). From statistical indices, smaller biases occur for S_CTRL, S_PBL and S_CLM (S_MIT, S_PBL_MIT, S_CLM_MIT) during DJF (JJA). In NDE, for DJF and JJA seasons the S_CTRL SD is closer to that of the the CMAP/CRU and the time correlation varies from 0.6 to 0.8.

Over NDE, the simulations capture the observed phase of the annual cycle of the air temperature, with most of the experiments (except S_Tiedke) presenting cold biases from January to October (Fig. 10b). The simulations reproduce the observed (CRU and UDEL) low values of SD, except for S_MIT and S_CLM_MIT in DJF. Most of the experiments present air temperature time correlations with CRU of 0.7 to 0.8 (Fig. 10b). A general analysis indicates S_CLM as the best configuration to simulate the annual cycle of precipitation over NDE, while S_MIT and S_CLM_MIT are slightly better for air temperature.

Fig. 9c shows that the simulations are able to reproduce the observed phase of the annual cycle of precipitation in La Plata Basin (LPB), i.e. the rainfall minimum (maximum) in August (October–April). The smallest biases occur in S_CLM_MIT from April-July and in S_CTRL from August-December. Fig. 9c indicates that the coupling of CLM with MIT scheme (in S_CLM_MIT) reduces the wet bias of the MIT scheme (in S_MIT). In general, during DJF there is an overestimate of the observed (CMAP and CRU) SD, and low correlation with CMAP, except in S_CTRL.

From CMAP and CRU data, in the subdomain near the border between Ecuador and northwestern Peru (AN1), the rainy season occurs from January to April (Fig. 9d). However, over AN1, which includes the steeper topography of the Andes Mountains, there are differences in both phase and amount of monthly rainfall between CMAP and CRU. The precipitation maximum occurs between February-March and March in CMAP and CRU, respectively. Moreover, the rainfall amount in CRU is greater than in CMAP throughout the year. Among the 5 analyzed subdomains, the rainfall in AN1 shows more spread in the simulated monthly mean values. In this subdomain, S_CLM and S_PBL (S_MIT, S_PBL_MIT and S_CLM_MIT) underestimate (overestimate) the precipitation throughout the year. S_CTRL and S_Tiedtke simulated precipitation amounts are closer to CMAP, but S_Tiedtke does not represent the observed phase of the annual cycle. In DJF, the SD is high in the observations, and only the simulations with the MIT convective scheme can reproduce this feature. In this season, the Grell and

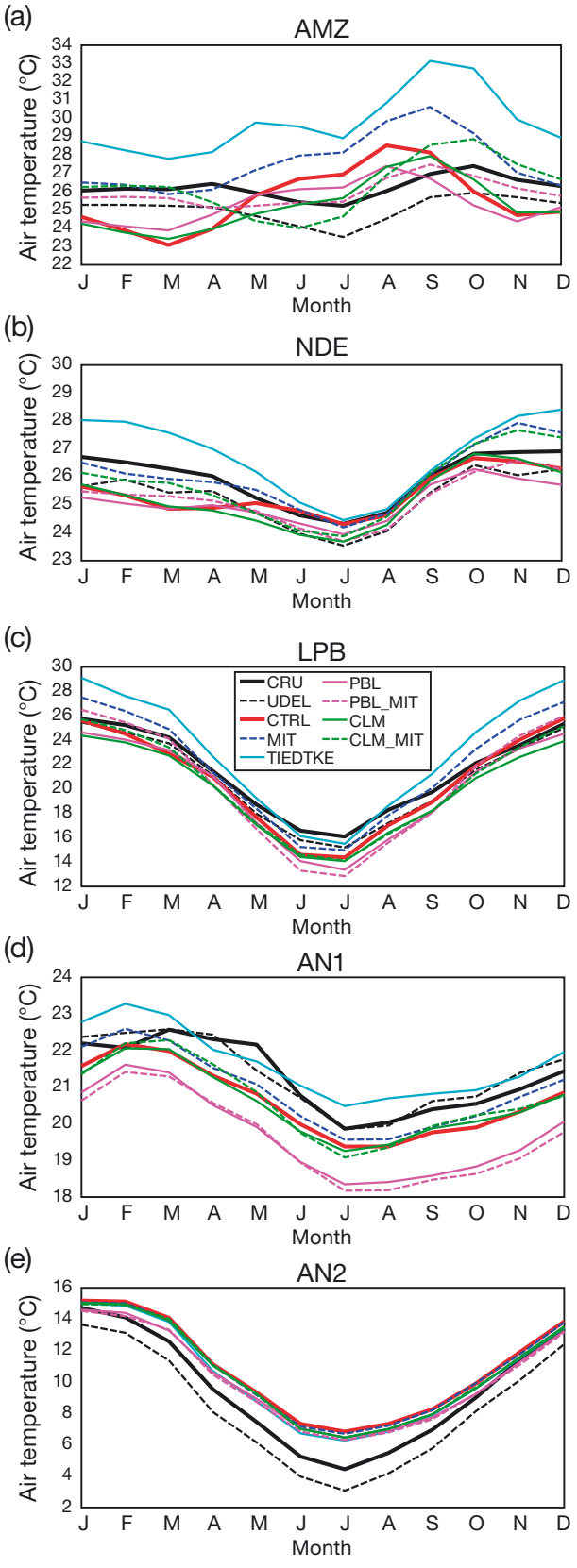

AMZ	MEAN	SD	BIAS	r
CRU	26.1 (25.5)	0.4 (0.6)	–	–
UDEL	25.3 (24.0)	0.4 (0.7)	−0.8 (−1.5)	0.9 (0.9)
S_CTRL	24.4 (27.4)	1.5 (1.1)	−1.7 (1.9)	0.7 (0.7)
S_MIT	26.4 (28.6)	1.0 (1.2)	0.3 (3.1)	0.7 (0.8)
S_TIEDTKE	28.6 (29.7)	1.2 (1.0)	2.5 (4.2)	0.6 (0.8)
S_PBL	24.5 (26.6)	0.9 (0.9)	−1.6 (1.1)	0.8 (0.7)
S_PBL_MIT	25.7 (25.8)	0.3 (0.9)	−0.4 (0.3)	0.8 (0.8)
S_CLM	24.3 (26.1)	1.0 (1.3)	−1.8 (0.6)	0.7 (0.7)
S_CLM_MIT	26.4 (25.2)	0.4 (1.6)	0.3 (−0.3)	0.7 (0.7)

NDE	MEAN	SD	BIAS	r
CRU	26.7 (24.5)	0.4 (0.4)	–	–
UDEL	25.9 (23.8)	0.6 (0.5)	−0.8 (−0.7)	0.8 (0.8)
S_CTRL	25.7 (24.6)	0.6 (0.4)	−1.0 (0.1)	0.7 (0.8)
S_MIT	26.7 (24.5)	0.9 (0.5)	0.0 (0.0)	0.7 (0.8)
S_TIEDTKE	28.1 (24.8)	0.5 (0.4)	1.4 (0.3)	0.7 (0.8)
S_PBL	25.3 (24.2)	0.5 (0.4)	−1.4 (−0.3)	0.7 (0.7)
S_PBL_MIT	25.7 (24.0)	0.5 (0.4)	−1.0 (−0.5)	0.7 (0.8)
S_CLM	25.7 (24.0)	0.5 (0.5)	−1.0 (−0.5)	0.6 (0.8)
S_CLM_MIT	26.5 (24.2)	0.8 (0.5)	−0.2 (−0.3)	0.6 (0.8)

LPB	MEAN	SD	BIAS	r
CRU	25.4 (17.0)	0.5 (1.6)	–	
UDEL	25.0 (16.1)	0.5 (1.5)	−0.4 (−0.9)	0.9 (1.0)
S_CTRL	25.3 (15.3)	1.1 (1.8)	0.1 (−1.7)	0.5 (0.8)
S_MIT	27.0 (16.0)	0.8 (1.9)	1.6 (−1.0)	0.3 (0.9)
S_TIEDTKE	28.5 (16.7)	1.0 (2.0)	3.1 (−0.3)	0.4 (0.9)
S_PBL	24.4 (14.4)	0.8 (1.6)	−1.0 (−2.6)	0.6 (0.8)
S_PBL_MIT	26.0 (14.0)	0.7 (1.8)	0.6 (−3.0)	0.5 (0.9)
S_CLM	24.0 (14.9)	0.9 (1.5)	−1.4 (−2.1)	0.6 (0.9)
S_CLM_MIT	25.2 (15.0)	0.6 (1.4)	−0.2 (−2.0)	0.6 (0.8)

AN1	MEAN	SD	BIAS	r
CRU	21.9 (20.2)	0.7 (0.8)	–	–
UDEL	22.2 (20.2)	0.8 (0.7)	0.3 (0.0)	0.7 (0.7)
S_CTRL	21.5 (19.6)	1.1 (0.8)	−0.4 (−0.6)	0.7 (0.6)
S_MIT	21.9 (19.8)	1.1 (0.8)	0 (−0.4)	0.7 (0.6)
S_TIEDTKE	22.7 (20.7)	1.2 (0.9)	0.8 (0.5)	0.7 (0.6)
S_PBL	20.8(18.6)	1.2 (1.0)	−1.1 (−1.6)	0.7 (0.6)
S_PBL_MIT	20.6 (18.4)	1.2 (1.0)	−1.3 (−1.8)	0.7 (0.6)
S_CLM	21.4 (19.5)	1.1 (0.8)	−0.5 (−0.7)	0.7 (0.6)
S_CLM_MIT	21.4 (19.4)	1.0 (0.8)	−0.5 (−0.8)	0.7 (0.7)

AN2	MEAN	SD	BIAS	r
CRU	14.1 (5.0)	0.9 (1.0)	–	–
UDEL	13.0 (3.7)	1.0 (1.2)	1.1 (−1.3)	0.9 (1.0)
S_CTRL	14.7 (7.1)	1.1 (0.8)	0.6 (2.1)	0.8 (0.9)
S_MIT	14.6 (7.0)	1.2 (0.9)	0.5 (2.0)	0.8 (0.9)
S_TIEDTKE	14.4 (6.6)	1.3 (0.9)	0.3 (1.6)	0.8 (0.9)
S_PBL	14.1 (6.8)	1.0 (0.8)	0.0 (1.8)	0.8 (0.9)
S_PBL_MIT	13.9 (6.6)	1.1 (0.8)	−0.2 (1.6)	0.8 (0.9)
S_CLM	14.5 (6.8)	1.1 (0.9)	0.4 (1.8)	0.8 (0.9)
S_CLM_MIT	14.4 (6.8)	1.2 (0.9)	0.3 (1.8)	0.8(0.9)

Fig. 10. Similar to Fig. 9, but for air temperature

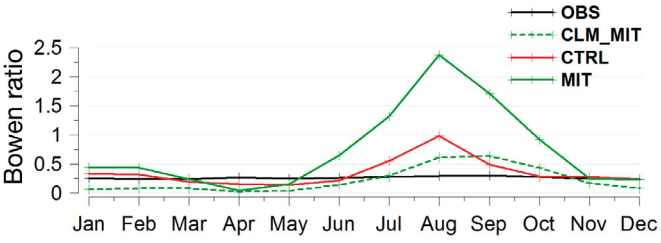

Fig. 11. Bowen Ratio (β) for S_CTRL, S_MIT and S_CLM_MIT experiments and observations in Amazon (see Section 2.2 for more details)

Tiedtke convective schemes simulate lower interannual variability than that observed.

In southern Chile (AN2), precipitation is conditioned by the meridional migration of the South Pacific Subtropical Anticyclone (Aceituno 1980), which moves northward in JJA, favoring precipitation. As shown by CMAP (Fig. 9e), JJA is the rainy season over AN2, as presented also by Reboita et al. (2010c) and Rojas (2006). The simulations reproduce the observed phase of the annual cycle of precipitation but, in general, overestimate it from June to November (Fig. 9e). The lowest rainfall bias occurs with S_Tiedtke and the highest biases in S_MIT and S_PBL_MIT. AN2 is the subdomain where the simulations present the highest correlations with CMAP, in DJF as well as JJA. In addition, in JJA the simulated SDs are closer to CMAP than during DJF. These indices indicate that the simulations better represent the observed interannual variability in AN2 during the rainy season.

The phases of the annual cycle of air temperature in LPB, AN1 and AN2 in the simulations are in accord with the CRU and UDEL data (Figs. 10c–e). Considering DJF, over the LPB (Fig. 10c), S_CTRL and S_CLM_MIT (S_Tiedke) present the lowest (highest) bias in air temperature. For the AN1 subdomain (Fig. 10d), S_PBL and S_PBL_MIT underestimate the air temperature compared to CRU, while other simulations are closer to this analysis. The simulations present positive bias over AN2 (Fig. 10e) during most of the year.

4. CONCLUSIONS

This study analyzed the best RegCM4.3 configurations for the simulation of the climate of SA. We carried out 7 simulations from January 1989 to January 2000. The control simulation (S_CTRL) used the Mixed1, Holtslag, and BATS schemes for cumulus convection, PBL and surface interactions, respectively. In the other simulations we changed these schemes using the new options of RegCM4.3, considering 3 groups: sensitivity to convection schemes (Mixed1, MIT and Tiedtke), sensitivity to planetary boundary layer (PBL) schemes (Holtslag and UW-PBL) and sensitivity to surface schemes (BATS and CLM). From these 3 groups, S_CTRL simulated the spatial pattern of the precipitation and its intensity with remarkable agreement with CMAP. However, the air temperature presents good agreement with observations when the MIT convective scheme is used (S_MIT, S_PBL_MIT, S_CLM_MIT). Therefore, we can conclude that the MIT convective scheme is important to climate studies that focus mainly on SA air temperature, while the Mixed1 scheme is recommended for precipitation (except in the Amazon region where S_CLM_MIT is better).

Simulations using the MIT convective scheme presented higher wet bias compared to CMAP than that with Mixed1 (Grell over the continent). The reason is that the MIT scheme overestimates evapotranspiration. Another interesting result is when the PBL scheme is changed from Holtslag to UW-PBL, the dry and wet biases, respectively, remain for the experiments with Mixed1 (S_PBL) and with MIT (S_PBL_MIT). Therefore, the convective scheme has greater control over precipitation than the PBL scheme. When CLM is coupled in the simulations, it contributes to decreases in evapotranspiration. Thus, (1) the dry bias increases in the experiment with Mixed1 (S_CLM) when it is compared to the experiment with Mixed1 and BATS (S_CTRL); and (2) the wet bias decreases in the experiment S_CLM_MIT (CLM with MIT) when it is compared to the experiment S_MIT (BATS with MIT). The combination of CLM and MIT produces the best simulation of air temperature over SA.

In the subdomain analysis, RegCM4.3 is able to simulate the phase and intensity of the precipitation and the annual cycles of air temperature in most of the subdomains. Some results need to be highlighted: Although the Tiedtke scheme does not have a realistic performance over a large part of SA, it presented good agreement with observations in the simulation of the annual cycle of precipitation over southern Chile. S_CLM has a more realistic representation of the rainy season over northeastern Brazil. On the other hand, S_CLM_MIT is the only simulation that produces an annual cycle of air temperature similar to that observed over Amazon. This last result can be associated with the better energy partition (latent and sensible heat fluxes) in the S_CLM_MIT simulation, which presents a Bowen Ratio lower <1, which is comparable to the observations. Over La Plata basin and northern Peru, S_CTRL simulates both precipitation

and air temperature well, providing good agreement with the observations.

Based on the whole analysis, we recommend the configurations of S_CTRL (with these schemes: Mixed1-cumulus convection, Holtslag-PBL, BATS-surface interactions), and S_CLM_MIT (with these schemes: MIT-cumulus convection, Holtslag-PBL, CLM-surface interactions) as the best configurations of RegCM4.3 for conducting the simulations of the CORDEX project over SA.

Acknowledgements. We thank the RegCM team (mainly Filippo Giorgi and Graziano Giuliani) and ECMWF, CRU and CMAP for the datasets. Thanks also to the CAPES/PROCAD-179/2007, CAPES-PROEX, and CNPq (307202/2011-12) for partial financial support and to the 3 anonymous reviewers whose suggestions helped us to improve the manuscript.

LITERATURE CITED

Aceituno P (1980) Relation entre la posicion del anticiclon subtropical y la precipitación en Chile. Project Report E.551.791, University of Chile, Santiago

Anthes RA (1977) A cumulus parameterization scheme utilizing a one-dimensional cloud model. Mon Weather Rev 105:270–286

Anthes RA, Hsie EY, Kuo YH (1987) Description of the Penn State/NCAR mesoscale model version 4 (MM4). Tech Note TN-282+STR, National Center for Atmospheric Research, Boulder, CO

Bowen IS (1926) The ratio of heat losses by conduction and evaporation from any surface. Phys Rev 27:779–789

Bretherton CS, McCaa JR, Grenier H (2004) A new parameterization for shallow cumulus convection and its application to marine subtropical cloud-topped boundary layers. I. Description and 1D Results. Mon Weather Rev 132: 864–882

Brohan P, Kennedy JJ, Harris I, Tett SFB, Jones PD (2006) Uncertainty estimates in regional and global observed temperature changes: a new dataset from 1850. J Geophys Res 111:D12106, doi:10.1029/2005JD006548

Chou SC, Nunes AMB, Cavalcanti IAF (2000) Extended range forecasts over South America using the regional eta model. J Geophys Res 105:10147–10160

da Rocha RP, Morales CA, Cuadra SV, Ambrizzi T (2009) Precipitation diurnal cycle and summer climatology assessment over South America: an evaluation of Regional Climate Model Version 3 simulations. J Geophys Res 114:D10108, doi:10.1029/2008JD010212

da Rocha RP, Cuadra SV, Reboita MS, Kruger LF, Ambrizzi T, Krusche N (2012) Effects of RegCM3 parameterizations on simulated rainy season over South America. Clim Res 52:253–265

Dee DP, Uppala SM, Simmons AJ, Berrisford P, and others (2011) The ERA-Interim reanalysis: configuration and performance of the data assimilation system. QJR Meteorol Soc 137:553–597

Dickinson RE, Errico RM, Giorgi F, Bates GT (1989) A regional climate model for the western United States. Clim Change 15:383–422

Dickinson RE, Henderson-Sellers A, Kennedy PJ (1993) Biosphere–Atmosphere Transfer Scheme (BATS) version 1E as coupled to the NCAR community climate model. Tech. Note NCAR/TN-3871STR, National Center for Atmospheric Research, Boulder, CO

Diro GT, Rauscher SA, Giorgi F, Tompkins AM (2012) Sensitivity of seasonal climate and diurnal precipitation over Central America to land and sea surface schemes in RegCM4. Clim Res 52:31–48

Emanuel KA (1991) A scheme for representing cumulus convection in large-scale models. J Atmos Sci 48:2313–2335

Emanuel KA, Zivkovic-Rothman M (1999) Development and evaluation of a convection scheme for use in climate models. J Atmos Sci 56:1766–1782

Fernandez JPR, Franchito SH, Rao VB (2006a) Simulation of summer circulation over South America by 2 regional climate models. I. Mean climatology. Theor Appl Climatol 86:247–260

Fernandez JPR, Franchito SH, Rao VB (2006b) Simulation of the summer circulation over South America by two regional climate models. II. A comparison between 1997/1998 El Niño and 1998/1999 La Niña events. Theor Appl Climatol 86:261–270.

Giorgi F, Marinucci MR (1991) Validation of a regional atmospheric model over Europe: sensitivity of wintertime and summertime simulations to selected physics parameterizations and lower boundary conditions. QJR Meteorol Soc 117:1171–1206

Giorgi F, Marinucci MR, Bates G (1993a) Development of a second generation regional climate model (RegCM2). I. Boundary layer and radiative transfer processes. Mon Weather Rev 121:2794–2813

Giorgi F, Marinucci MR, Bates G, De Canio G (1993b) Development of a second generation regional climate model (RegCM2). II. Convective processes and assimilation of lateral boundary conditions. Mon Weather Rev 121: 2814–2832

Giorgi F, Bi X, Pal JS (2004) Mean, interannual variability and trends in a regional climate experiment over Europe. I. Present day climate (1960–1990). Clim Dyn 22:733–756

Giorgi F, Jones C, Asrar G (2009) Addressing climate information needs at the regional level: the CORDEX framework. World Meterol Organ Bull 58:175–183

Giorgi F, Coppola E, Solmon F, Mariotti L and others (2012) RegCM4: model description and preliminary tests over multiple CORDEX domains. Clim Res 52:7–29.

Grell GA (1993) Prognostic evaluation of assumptions used by cumulus parameterizations. Mon Weather Rev 121: 764–787

Grenier H, Bretherton CS (2001) A moist PBL parameterization for large scale models and its application to subtropical cloud-topped marine boundary layers. Mon Weather Rev 129:357–377

Güttler I, Brankovic C, O'Brien TA, Coppola E, Grisogono B, Giorgi F (2013) Sensitivity of the regional climate model RegCM4.2 to planetary boundary layer parameterization. Clim Dyn, doi:10.1007/s00382-013-2003-6

Hastenrath S (1991) Climate Dynamics of the Tropics. Kluwer Academic Publishers, Dordrecht

Hastenrath S, Heller L (1977) Dynamics of climatic hazards in northeast Brazil. QJR Meteorol Soc 103:77–92

Holtslag A, de Bruijn E, Pan HL (1990) A high resolution air mass transformation model for short-range weather forecasting. Mon Weather Rev 118:1561–1575

Krüger LF, da Rocha RP, Reboita MS, Ambrizzi T (2012) RegCM3 nested in HadAM3 scenarios A2 and B2: projected changes in extratropical cyclogenesis, temperature and precipitation over the South Atlantic Ocean. Clim Change 113:599–621.

Legates DR, Willmott CJ (1990) Mean seasonal and spatial variability in global surface air temperature. Theor Appl Climatol 41:11–21

Loveland TR, Reed BC, Brown JF, Ohlen DO, Zhu Z, Yang L, Merchant JW (2000) Development of a global land cover characteristics database and IGBP DISCover from 1 km AVHRR data. Int J Remote Sens 21:1303 – 1365

Marengo JA, Liebmann B, Grimm AM, Misra V and others (2012) Recent developments on the South American monsoon system. Int J Climatol 32:1–21

Marengo JA, Ambrizzi T, da Rocha RP, Alves LM and others (2010) Future change of climate in South America in the late twenty-first century: intercomparison of scenarios from three regional climate models. Clim Dyn 35: 1073–1097

Martínez-Castro D, da Rocha RP, Bezanilla A, Alvarez L, Fernández JPR, Silva Y, Arritt R (2006) Sensitivity studies of the RegCM-3 simulation of summer precipitation, temperature and local wind field in the Caribbean Region. Theor Appl Climatol 86:5–22

Menéndez CG, Saulo AC, Li ZX (2001) Simulation of South American wintertime climate with a nesting system. Clim Dyn 17:219–231

Misra V, Dirmeyer PA, Kirtman BP, Juang HMH, Kanamitsu M (2002) Regional simulation of interannual variability over South America. J Geophys Res 107 (D20), doi:10.1029/2001JD900216

Negrón Juárez RI, Hodnett MG, Fu R, Goulden ML, von Randow C (2007) Control of dry season evapotranspiration over Amazonian forest as inferred from observations at a southern Amazon forest site. J Clim 20:2827–2839

Nicolini M, Salio P, Katzfey JJ, McGregor JL, Saulo AC (2002) January and July regional climate simulation over South American. J Geophys Res 107:4637, doi:10.1029/2001JD000736

Nobre PA, Moura D, Sun L (2001) Dynamical downscaling of seasonal climate prediction over Nordeste Brazil with ECHAM3 and NCEP's Regional Spectral Models at IRI. Bull Am Meteorol Soc 82:2787–2796

Nunes AMB, Roads JO (2005) Improving regional model simulations with precipitation assimilation. Earth Interact 9:1–44

Nuñez MN, Solman SA, Carbré MF (2009) Regional climate change experiments over southern South America. II. Climate change scenarios in the late twenty-first century. Clim Dyn 32:1081–1095

O'Brien TAO, Chuang PY, Sloan LC, Faloona IC, Rossiter DL (2012) Coupling a new turbulence parametrization to RegCM adds realistic stratocumulus clouds. Geosci Model Dev 5:989–1008

Oleson KW, Dai Y, Bonan G, Bosilovich M and others (2004) Technical description of the community land model. Tech Note NCAR/TN-461+STR, National Center for Atmospheric Research NCAR, Boulder, CO

Oleson KW, Niu GY, Yang ZL, Lawrence DM and others (2008) Improvements to the community land model and their impact on the hydrologic cycle. J Geophys Res 113: G01021, doi:10.1029/2007JG000563

Pal JS, Giorgi F, Bi X, Elguindi N, and others (2007) Regional climate modeling for the developing world: the ICTP RegCM3 and RegCNET. Bull Am Meteorol Soc 88: 1395–1409

Rauscher SA, Seth A, Liebmann B, Qian JH, Camargo SJ (2007) Regional climate model–simulated timing and character of seasonal rains in South America. Mon Weather Rev 135:2642–2657

Reboita MS, da Rocha RP, Ambrizzi T, Shigetoshi S (2010a) South Atlantic Ocean cyclogenesis climatology simulated by regional climate model (RegCM3). Clim Dyn 35: 1331–1347

Reboita MS, da Rocha RP, Ambrizzi T, Caetano E (2010b) An assessment of the latent and sensible heat flux on the simulated regional climate over Southwestern South Atlantic Ocean. Clim Dyn 34:873–889

Reboita MS, Gan MA, da Rocha RP, Ambrizzi T (2010c) Regimes de precipitação na América do Sul: uma revisão bibliográfica. Rev Bras Med 25:185–204

Reboita MS, da Rocha RP, Krüger LF (2013) Climate forecast to southern Minas Gerais state. Scientific Report 473153/2010-6, CNPq, Brasília

Reynolds RW, Rayner NA, Smith TM, Stokes DC, Wang W (2002) An improved in situ and satellite SST analysis for climate. J Clim 15:1609–1625

Rocha HR, Manzi AO, Cabral OM, Miller SD, and others (2009) Patterns of water and heat flux across a biome gradient from tropical forest to savanna in Brazil. J Geophys Res 114:G00B12, doi:10.1029/2007JG000640

Rojas M (2006) Multiply nested regional climate simulation for southern South America: sensitivity to model resolution. Mon Weather Rev 134:2208–2223

Sellers PJ, Dickinson RE, Randall DA, Betts AK and others (1997) Modeling the exchanges of energy, water, and carbon between continents and the atmosphere. Science 275:502–509

Sen OL, Wang Y, Wang B (2004) Impact of Indochina deforestation on the East-Asian summer monsoon. J Clim 17: 1366–1380

Seth A, Rojas M (2003) Simulation and sensitivity in a nested modeling system for tropical South America. I. Reanalyses boundary forcing. J Clim 16:2437–2453

Seth A, Rauscher SA, Camargo SJ, Qian JH, Pal JS (2007) RegCM3 regional climatologies for South America using reanalysis and ECHAM global model driving fields. Clim Dyn 28:461–480

Solman SA, Sanchez E, Samuelsson P, da Rocha RP and others (2013) Evaluation of an ensemble of regional climate model simulations over South America driven by the ERA-Interim reanalysis: model performance and uncertainties. Clim Dyn 41:1139–1157

Steiner AL, Pal JS, Giorgi F, Dickinson RE, Chameides WL (2005) Coupling of the common land model (CLM0) to a regional climate model (RegCM). Theor Appl Climatol 82:225–243

Steiner AL, Pal JS, Rauscher SA, Bell JL and others (2009) Land surface coupling in regional climate simulations of the West Africa monsoon. Clim Dyn 33(6):869-892,

Tawfik AB, Steiner AL (2011) The role of soil ice in land–atmosphere coupling over the United States: a soil moisture precipitation winter feedback mechanism. J Geophys Res 116:D02113, doi:10.1029/2010JD014333

Tiedtke M (1989) A comprehensive mass-flux scheme for cumulus parameterization in large-scale models. Mon Weather Rev 117:1779–1800

Vera C, Higgins W, Amador J, Ambrizzi T and otherss (2006) Toward a unified view of the American monsoon systems. J Clim 19:4977–5000

Xie P, Arkin PA (1997) Global precipitation: a 17-year monthly analysis based on gauge observations, satellite estimates, and numerical model outputs. Bull Am Meteorol Soc 78:2539–2558

Zeng X, Zhao M, Dickinson RE (1998) Intercomparison of bulk aerodynamic algorithms for the computation of sea surface fluxes using TOGA COARE and TAO data. J Clim 11:2628–2644

Editorial responsibility: Filippo Giorgi, Trieste, Italy

Submitted: June 5, 2013; Accepted: May 2, 2014
Proofs received from author(s): July 17, 2014